Ab Initio Investigation on Cu/Cr Codoped Amorphous Carbon Nanocomposite Films with Giant Residual Stress Reduction

Xiaowei Li,* Peng Guo, Lili Sun, Aiying Wang,* and Peiling Ke

Key Laboratory of Marine Materials and Related Technologies, Key Laboratory of Marine Materials and Protective Technologies of Zhejiang Province, Ningbo Institute of Materials Technology and Engineering, Chinese Academy of Sciences, Ningbo 315201, People's Republic of China

ⓈSupporting Information

ABSTRACT: Amorphous carbon films (a-C) codoped by two metal elements exhibit the desirable combination of tribological and mechanical properties for widely potential applications, but are also prone to catastrophic failure due to the inevitable residual compressive stress. Thus far, the residual stress reduction mechanism remains unclear due to the insufficient understanding of the structure from the atomic and electronic scale. In this paper, using ab initio calculations, we first designed a novel Cu/Cr codoped a-C film and demonstrated that compared with pure and Cu/Cr monodoped cases, the residual stress in Cu/Cr codoped a-C films could be reduced by 93.6% remarkably. Atomic bond structure analysis revealed that the addition of Cu and Cr impurities in amorphous carbon structure resulted in the critical and significant relaxation of distorted C−C bond lengths. On the other hand, electronic structure calculation indicated a weak bonding interaction between the Cr and C atoms, while the antibonding interaction was observed for the Cu−C bonds, which would play a pivot site for the release of strain energy. Those interactions combined with the structural evolution could account for the drastic residual stress reduction caused by Cu/Cr codoping. Our results provide the theoretical guidance and desirable strategy to design and fabricate a new nanocomposite a-C films with combined properties for renewed applications.

KEYWORDS: residual stress, bond structure, codoping, amorphous carbon, ab initio calculation
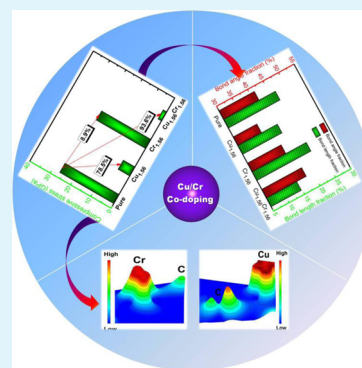
1. INTRODUCTION

Amorphous carbon (a-C) materials have aroused significant attention owing to their unique structures and superior mechanical, chemical, electronic and magnetic properties,[1−3] making them a strong candidate as a protective coating in the fields of cutting tools, modulus, automobile and magnetic disk storage devices to minimize the mechanical wear and corrosion.[4−6] However, it is still necessary to overcome the current a-C materials limitations for wider applications, as exemplified by the inevitable high residual compressive stress, which deteriorates the adhesive strength between the films and substrate and ultimately leads to catastrophic failure of the coated surface. Introducing metal elements into a-C films has been proved to be effective way to reduce the residual compressive stress effectively by the pivot site of metal nanocrystallites for structure relaxation,[7] substitution of strong C−C bonds by weak Me−C bonds,[8] or the promoted graphitization of C-sp[2] bonds.[9]

Especially, two or more metal elements codoping has been taken into account recently to overcome these barriers and explore new functions conveyed by multiple nanostructures coexisting in carbon films. For example, Liu et al.[10−12] recently reported that the Ti/Al codoped a-C films exhibited low residual stress, high hardness, good toughness, as well as low friction coefficient and wear rate, which was attributed to the formation of a graphitized transfer layer. Moreover, when Ti

was replaced by Si, a near-frictionless and superelastic behavior but low hardness was obtained in Si/Al codoped a-C:H films, due to the dual nanocompsite structures combined with fullerene-like clusters in carbon matrix.[13] So, codoping two metal elements in a-C films could provide the desirable combination of tribological and mechanical properties. Nevertheless, the novel Cu/Cr codoped nanocomposite carbon matrix has also never been mentioned. Most importantly, because of the difficulties in direct observation of structural evolution by experiments with atomic and electronic scale, the dependence of residual stress on microstructure has not been fully understood yet, which is indispensable for exploring the stress reduction mechanism. Ab initio calculations provide a powerful tool to capture atomic and electronic details and gain a deeper insight into the stress reduction mechanism of metal codoped a-C films.[14,15]

In the present study, we reported the first investigation on the novel Cu/Cr codoped a-C films using ab initio calculations based on density functional theory (DFT). The structure models were generated from liquid quench containing 64 atoms. The effect of Cu/Cr codoping on the residual stress was focused in terms of the evolution of atomic bond structure

including bond angles, bond lengths and bonding feature. The results showed that, in comparison with those pure and Cu/Cr monodoped a-C films, the Cu/Cr codoped case exhibited an extremely low residual compressive stress due to the relaxation of highly distorted bond lengths and the formation of weak Cr−C and Cu−C bonds. If one notes the optimized designing with the selected codoped metal characteristics, our results present a new straightforward strategy to tailor the a-C films with low residual stress and other novel physical and chemical properties.

2. COMPUTATIONAL DETAILS

All the calculations were carried out using the Vienna ab initio simulation package[16,17] with a cutoff energy of 500 eV and a generalized gradient approximation with the Perdew−Burke−Ernzerhof parametrization.[18] The initial configuration contained 64 atoms in a simple cubic supercell with constant volume and under periodic boundary conditions throughout the simulation, which has been proved to be suitable and accurate to reveal the characteristics of a-C films and also save the required computation time.[15,19] To obtain Cu/Cr codoped a-C films, a two-step process composed of melt-quenching by ab initio molecular dynamics (AIMD) simulation and geometric optimization (GO) was used, which has been demonstrated to give a good description of a-C materials and revealed the intrinsic relation between the structure and properties.[15,19,20]

Figure 1 shows the schematic diagram of the calculated process to obtain the Cu/Cr codoped a-C films. During the AIMD simulation, the initial sample was first equilibrated at 8000 K for 1 ps to become completely liquid state and eliminate its correlation to the initial configuration using *NVT* ensemble with a Nose thermostat for temperature-control and a time step of 1 fs, which was confirmed by calculating the radial distribution function (RDF) of the samples; then,
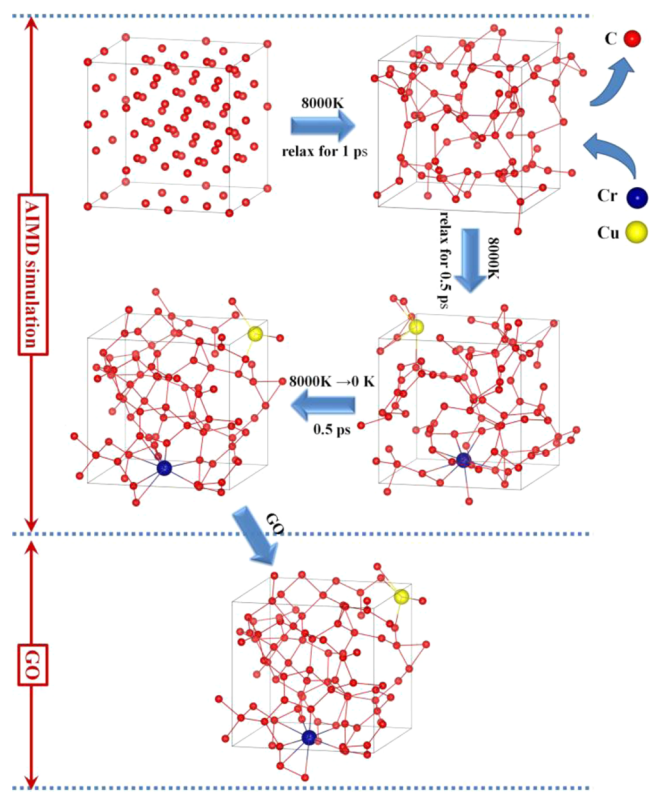
Figure 1. Schematic diagram to visually present the calculated process for obtaining the Cu/Cr codoped a-C films, in which red, yellow, and blue colors indicate the C, Cu and Cr atoms, respectively.

the sample was quenched from 8000 to 1 K at cooling rate of 1.6×10^{16} K/s. For the subsequent GO of amorphous structure, a full relaxation of the atomic positions based on conjugated gradient method[21] was repeated until the Hellmann−Feynman force on each atom was below 0.01 eV/Å, and the self-consistent loop was created using an energy convergence criterion of 10^{-5} eV; the Γ-only *k*-point was used to sample the Brillouin zone. To check the *k*-point convergence on amorphous structure, a fully converged calculation with a grid of $4 \times 4 \times 4$ points (64 *k*-points) was performed. When the Γ point only was used, the absolute error of average binding energy of per atom was found to be accurate to better than 0.004 eV compared to the fully converged calculation with 64 *k*-points.

In the designed Cu/Cr codoped amorphous structure, because we focused on the small amount of doped metal concentrations to avoid the giant deterioration of other mechanical and tribological properties dominated by the interlink amorphous carbon matrix, the total concentrations for Cu/Cr were selected ranging from 3.13 to 7.81 at. % with different Cu/Cr ratio, corresponding to 2, 3, 4 and 5 atoms in 64-atom models, respectively. To provide more representative models of the real metal doped film than the direct substitution of carbon by metal atoms in pregenerated pure carbon networks, Cu and Cr atoms were introduced by substituting carbon atoms in the liquid carbon state with a external equilibrium at 8000 K for 0.5 ps.[19] For comparison, pure and Cu/Cr monodoped cases with Cu or Cr concentrations of 1.56−7.81 at. % were also involved. Then, the RDF, hybridization fraction, residual compressive stress, and the bond structure were evaluated.

3. RESULTS AND DISCUSSION

The RDF, $g(r)$, is proportional to the density of atoms at a distance r from another atom, which is a very important parameter for structural characterization of amorphous materials, and it is computed by the formula

$$g(r) = \frac{dN}{\rho \cdot 4\pi r^2 dr} \tag{1}$$

where ρ is the average density of system, dN is the number of atoms from r to $r + dr$. Before characterizing the structure of Cu/Cr codoped a-C films, the RDF, $g(r)$, in the films with high metal concentration was analyzed first to define the Cu, Cr and C atoms being bonded or nonbonded with each other, as shown in Figure 2. The distance to the first minimum in RDF (see inset values of Figure 2) was set as the curoff distance, R_{cut}, for C−C, C−Cu, Cu−Cu, C−Cr, Cr−Cr and Cu−Cr bonds.[22,23]

Figure 3 shows the final atomic structures of Cu/Cr codoped a-C films with different Cu/Cr concentrations using the precalculated cutoff distance to determine the nearest neighbor atoms. Pure and Cu/Cr monodoped a-C films are also considered. It is worth noting that compared with the pure a-C film, doping Cu and/or Cr into carbon matrix causes the increase of density and tetra-coordinated C fraction. For pure a-C film, the tetra-coordinated C fraction in the network (Figure 3a) is 56.2%, which is consistent with previous work.[24] In Cu doped a-C films (Figure 3b−d),[22] the tetra-coordinated C hybridized structure with Cu concentration increases gradually, because the doped Cu atoms easily bonding with three-coordinated C atoms around the doped position. In particular, Figure 3d shows that the Cu atoms in the films with high Cu concentration could cluster with each other due to the weak Cu−C bond.[25] For the Cr doped a-C films (Figure 3e−g),[15] the tetra-coordinated C fraction increases first and then decreases, and the formation of many highly distorted five-coordinated C atoms in the films with higher Cr concentration could account for the change of hybridized structure. However,
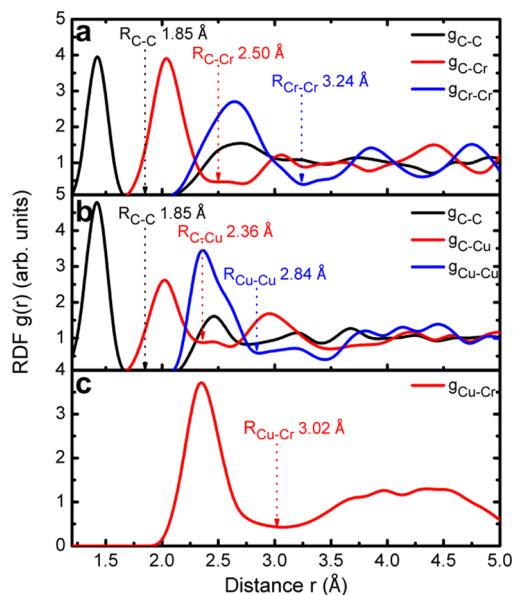
Figure 2. RDF of (a) Cu 39 at. % monodoped, (b) Cr 39 at. % monodoped and (c) Cu/Cr codoped a-C films with Cu and Cr concentrations of 39 at. % separately, where the inset values are the R_{cut} values for the C−C, C−Me, and Me−Me bonds.
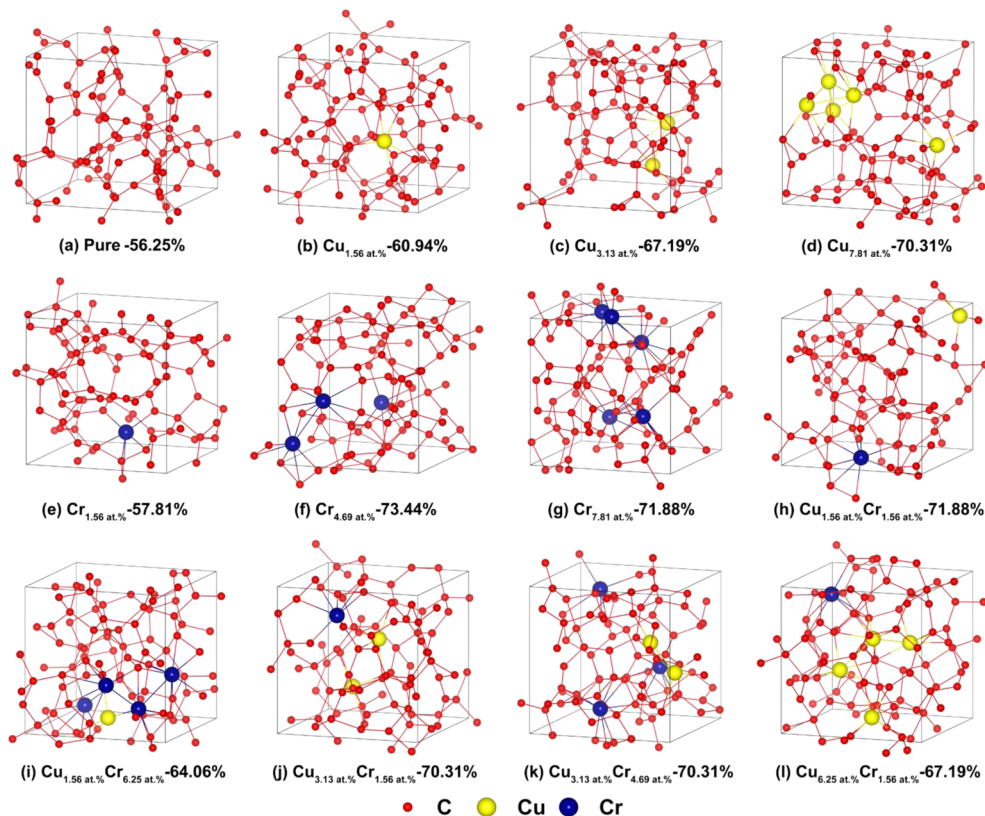
existed in each case compared with the Cu doped a-C film with Cu 7.81 at. % (Figure 3d).

Figure 4 shows the RDF spectra of pure and Cu/Cr codoped a-C films with different Cu/Cr concentrations, in which the
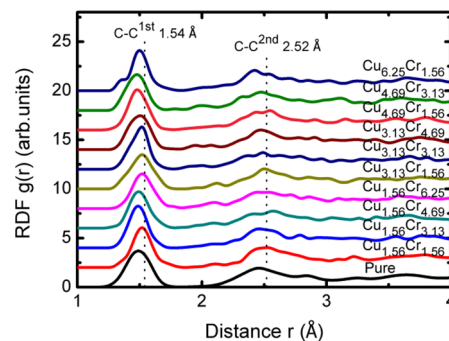

Figure 4. RDF spectra of pure and Cu/Cr codoped a-C films. The vertical dotted lines represent the 1st and 2nd nearest peak positions of crystalline diamond. The subscript is the concentration of doped metal atoms in the film.

vertical dotted lines represent the first and second nearest peak positions of crystalline diamond. It reveals that for each case the film shows the typical amorphous character, that is long-range disorder and short-range order. For pure a-C film, the first and second nearest neighbor peak are located at 1.50 and 2.46 Å, respectively. As known that the first peak is related with the atomic bond lengths, and the second peak correlates with both the bond angles and bond lengths. However, after the addition of Cu/Cr into amorphous carbon matrix, the positions of the

after doping Cu and Cr into carbon matrix simultaneously, the structure seems to be modified seriously, as illustrated in Figure 3h−l, which will induce the significant change of properties. In addition, it can be observed that there is no obvious Cu cluster


Figure 3. Atomic structures of (a) pure, (b−d) Cu doped, (e−g) Cr doped and (h−l) Cu/Cr codoped a-C films, in which the numbers are the tetra-coordinated C fractions in each film, and red, yellow and blue colors indicate the C, Cu and Cr atoms, respectively.
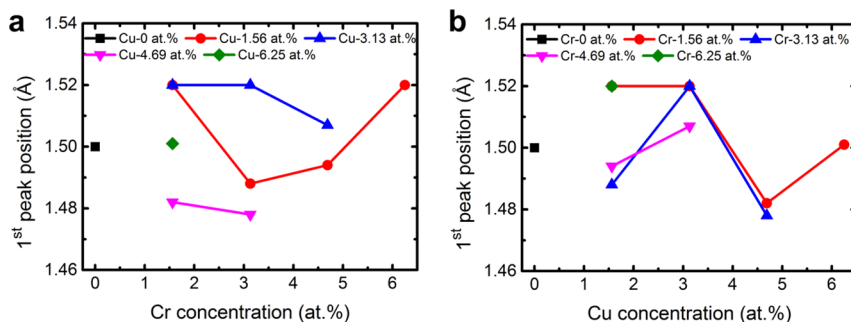
Figure 5. 1st peak position as a function of (a) Cr or (b) Cu concentration in Cu/Cr codoped a-C films.

first and second nearest neighbor peaks in the films are deviated from that of pure a-C film obviously as shown in Figure 5, demonstrating the evolution of atomic bond structure. Taking the film with Cu 1.56 at. % and Cr 1.56 at. % for example, the first peak increases to 1.52 Å from 1.50 Å of pure case (Figure 5), indicating the relaxation of distorted bond lengths and thus suggesting the reduction of residual stress. Nevertheless, the bond structure needs to be further analyzed in order to clarify the relation between the structure and properties.
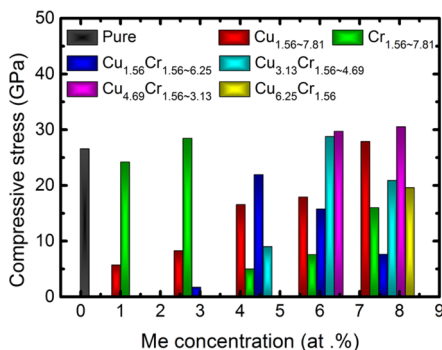
Figure 6. Compressive stress of pure, Cu/Cr mono- and codoped a-C films as a function of Me concentrations. The subscript is the concentration of doped metal atoms in the film.

The dependence of the calculated residual compressive stress on Cu/Cr concentrations is illustrated in Figure 6. The stress, σ, is computed by the equations

$$P = \frac{P_{xx} + P_{yy} + P_{zz}}{3} \tag{2}$$

$$\sigma = \frac{3}{2}P \tag{3}$$

where P is the hydrostatic pressure, P_{xx}, P_{yy} and P_{zz} are the diagonal components of the stress tensor; the pressure, P, is converted to the biaxial stress, σ, by multiplying the pressure by a factor of 1.5, according to the method of McKenzie (eqs 3).[26,27] In case of the pure a-C film, a high residual compressive stress about 26.6 GPa is estimated. With introducing Cu atoms into a-C films, the compressive stress as a function of Cu concentration decreases quickly and then increases; when the Cu concentration is 1.56 at. %, the minimal residual compressive stress of about 5.7 GPa is obtained, which is reduced by 78.5% compared with the pure case. Similar results have been confirmed by experiment.[25] For Cr doped a-C films,

the lowest compressive stress of about 5.0 GPa is measured as the Cr concentration is 4.69 at. %, while the further incorporation of Cr up to 7.81 at. % induces the compressive stress increased to 16.0 GPa. The evolution in the residual stress of a-C films by Cr incorporation is consistent with the previous experimental results.[28] Taking the benefits from the simulation, nevertheless, noted that the drastic evolution of residual stress is observed after introducing Cu/Cr into a-C films simultaneously. As the concentrations of codoped Cu and Cr atoms are all 1.56 at. %, the film exhibits the lowest residual stress about 1.7 GPa. By contrast with pure a-C case, codoping Cu and Cr could significantly reduce the residual stress by 93.6%, while in Cu/Cr monodoped cases the compressive stress only drops by 78.5% or 81.4%, respectively.

To elucidate the giant stress reduction mechanism caused by Cu/Cr codoping, more direct evidence for the atomic bond structure including both the bond angle and length distributions are collected first. Figure 7 shows the calculated results of both the bond angle and length distributions for the Cu/Cr codoped a-C film with Cu 1.56 at. % and Cr 1.56 at. % in which the lowest residual stress is observed (Figure 6). For comparison, the case for pure a-C film is also considered. In Figure 7a, the total bond angle distribution is composed of the bond angle distributions for all combinations, as shown in Figure 7b,c; compared with pure case, the total bond angle distribution in Cu/Cr codoped film shifts obviously toward the small bond angles around 70° (Figure 7a), which are contributed by the existence of the C−Cu−C, C−C−Cu, C−Cr−C and C−C−Cr bond angles shown in Figure 7c. The total bond length distribution in Figure 7d mainly consists of C−C, C−Cr and C−Cu bond lengths (Figure 7e,f); in particular, a small and wide peak located at around 2.13 Å is generated in the total bond length distribution, which originates from C−Cu and C−Cr bonds because they are longer than C−C bond (Figure 7f).

Li et al.[29] revealed that the distortion of both bond angles (<109.5°) and bond lengths (<1.42 Å) in carbon network was the key factor for the high level of residual compressive stress. Therefore, the C−C−C bond angles and C−C bond lengths in Cu/Cr codoped a-C film were particularly focused on to in order to gain the fractions of distorted bond angles and bond lengths, respectively, which are illustrated Figure 7b,e. The black vertical dotted lines In Figure 7b represent the equilibrium bond angle of 120° for graphite and 109.5° for the crystalline diamond. The equilibrium bond length of stable sp^2 and sp^3 C−C bonds are 1.42 and 1.54 Å separately (the red vertical dotted lines in Figure 7e). First, the C−C−C bond angle distribution of Cu/Cr codoped a-C film (Figure 7b) shows a peak at approximately 109.5°, demonstrating the
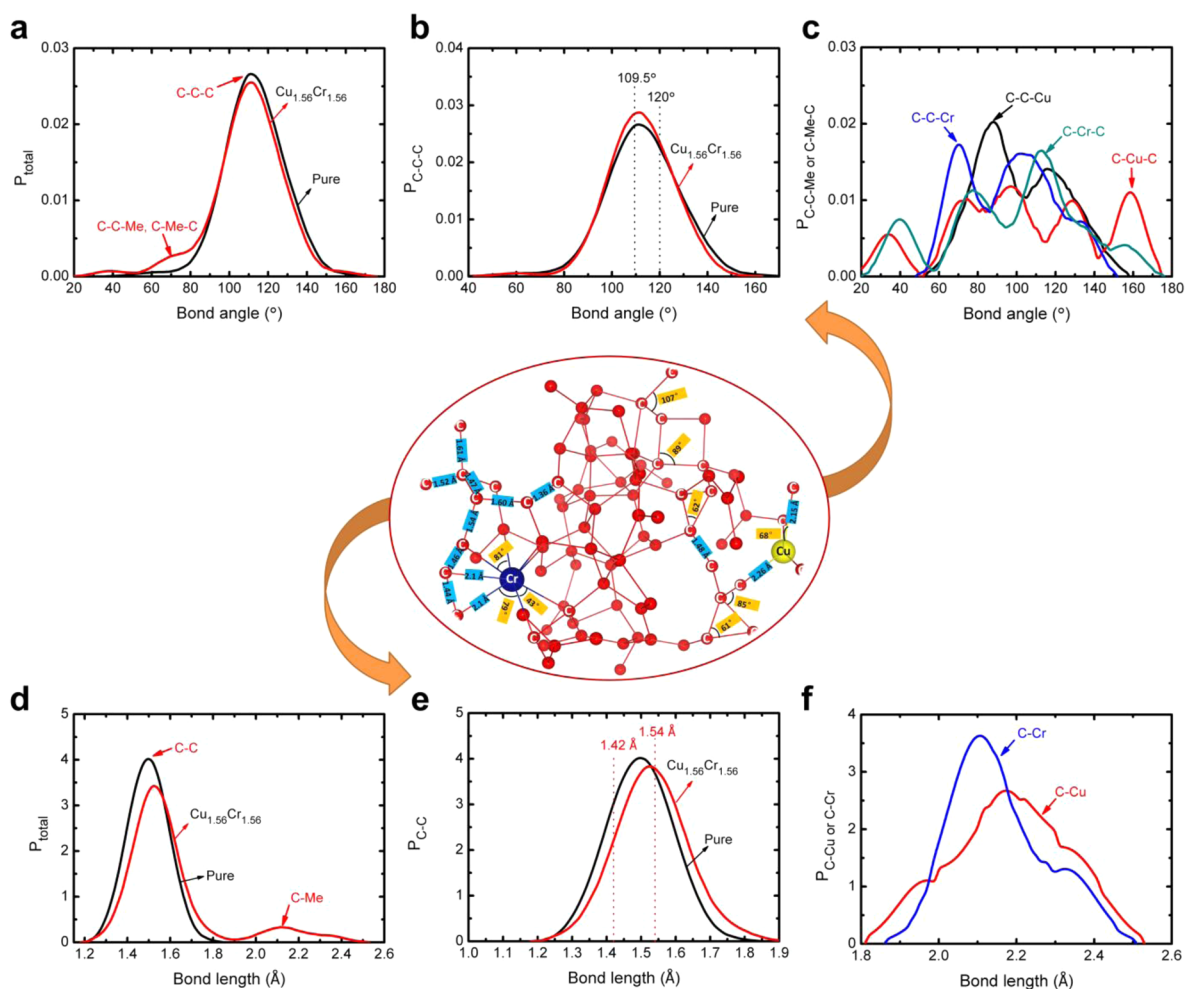
Figure 7. Atomic bond structure of pure, Cu/Cr codoped a-C films. (a) Total bond angle distributions being composed of the bond angle distributions for all combinations; (b) bond angle distributions of C−C−C, $P_{C−C−C}$, in which the black vertical dotted lines represent the stable bond angles of 120° for graphite and the one of 109.5° for diamond; (c) combined distributions of the bond angles containing Me and C atoms; (d) total bond length distribution being composed of C−C and C-Me bond lengths; (e) bond length distributions of C−C, $P_{C−C}$, in which the red vertical dotted lines represent the stable bond lengths of 1.42 and 1.54 Å for stable sp^2 and sp^3 C−C bonds, respectively; (f) combined distributions of the C−Cr and C−Cu bond lengths. The subscript is the concentration of doped metal atoms in the film.

prominent contribution from the tetra-coordinated atoms, and the peak position with the Cu/Cr codoping has no obvious change. Nevertheless, the peak position of the C−C bond length distribution in Figure 7e deviates to 1.54 Å distinctly, which is related to the change of tetra-coordinated C fraction (Figure 3).

By integrating the C−C−C bond angle and C−C bond length distributions (Figure 7b,e), the fractions of distorted bond angles (<109.5°) and bond lengths (<1.42 Å) in Cu/Cr codoped a-C film with Cu 1.56 at. % and Cr 1.56 at. % are thus deduced separately, as shown in Figure 8. The calculations for pure, Cu (1.56 at. %) and Cr (1.56 at. %) monodoped a-C films are also carried out for comparison. Figure 8 shows that in pure a-C film the fractions of distorted bond angles (<109.5°) and bond lengths (<1.42 Å) are 41.4% and 21.7%, respectively. After monodoping Cu 1.56 at. % into a-C film, the reduction of compressive stress attributes to the simultaneous relaxation of both the distorted bond lengths and bond angles, which are 37.6% and 17.7% separately; even if doping Cr 1.56 at. % into a-C film causes the distorted bond lengths increased to 22.4%, the fraction of highly distorted C−C−C bond angles decreases to 40.9%. This opposite and slight change in the distorted
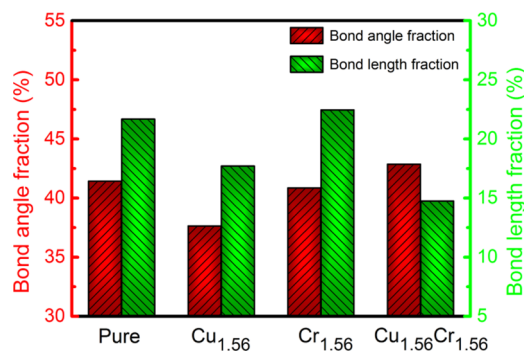

Figure 8. Fractions of distorted bond angles (<109.5°) and bond lengths (<1.42 Å) in pure, Cu/Cr mono- and codoped a-C films. The subscript is the concentration of doped metal atoms in the film.

atomic bond structure leads to the mediate change of residual stress, as illustrated in Figure 6. Nevertheless, with codoping Cu 1.56 at. % and Cr 1.56 at. % into a-C films, the synergistic effect of Cu and Cr atoms causes the distorted bond angles increased to 42.9% by comparing with Cu/Cr monodoped cases, while the fraction of distorted C−C bond lengths decreases

drastically to 14.7%, which contributes to the significant change of residual stress shown in Figure 6.

In addition, the evolution of electronic structure brought by Cu/Cr codoping is also of great importance for providing the further insight for the residual stress reduction mechanism. To analyze the constitution of valence band (VB) and conduction bond (CB), we first perform the spin resolved density of states (DOS) and projected density of states (PDOS) on the C, Cu and Cr atoms in the Cu/Cr codoped a-C film with Cu 1.56 at. % and Cr 1.56 at. %, as shown in Figure 9. It shows that VB
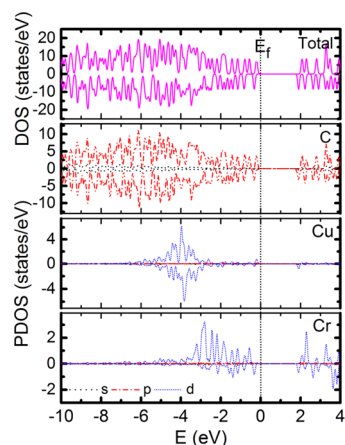
Figure 9. DOS and PDOS projected on the C, Cu and Cr atoms in the Cu/Cr codoped a-C film with Cu 1.56 at. % and Cr 1.56 at. %.

mainly consists of Cu 3d, Cr 3d, C 2s and C 2p states. The obvious hybridization in VB is observed between the Cu 3d or Cr 3d and C 2p states. CB is mainly composed of Cr 3d and C 2p states. Moreover, the Cu 3d and Cr 3d states in VB shift upward to near the Femi energy level compared with Cu/Cr monodoped case, attributing to the effect of Cu/Cr codoping (see Supporting Information Figure S1 and Figure S2).

The charge density of Cu/Cr codoped a-C film with Cu 1.56 at. % and Cr 1.56 at. % is examined. As shown in Figure 10a,
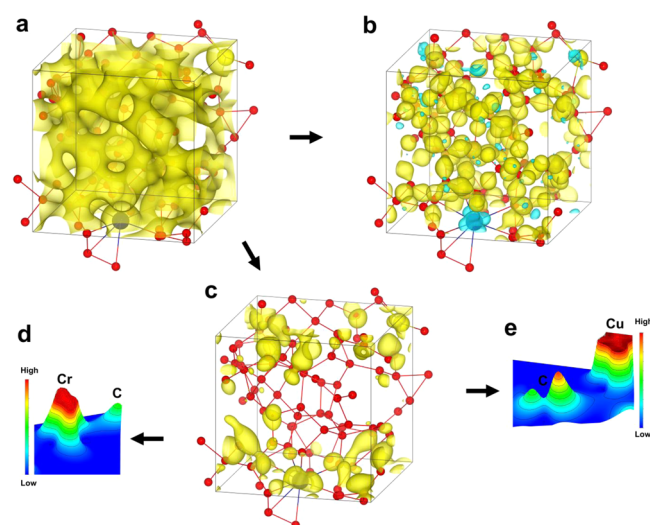
Figure 10. (a) Charge density, (b) charge density difference, (c) HOMO image, (d) 3D view of the HOMO charge density for Cr−C and (e) 3D view of the HOMO charge density for Cu−C bond in Cu/Cr codoped a-C film with Cu 1.56 at. % and Cr 1.56 at. %.

Cu or Cr and C atoms are connected by the charge distribution, which is the typical feature of covalent bond. Moreover, due to the electronegativity difference between Cu or Cr and C atoms, the charge of Cu and Cr atoms obviously shifts to neighboring C atoms (Figure 10b). The highest occupied molecular orbital (HOMO) characteristics in the films not only dominate the films stability, but also contribute to the films rigidity except the tetra-coordinated C fraction, so they are further analyzed. The PDOS (Figure 9) reveals that HOMO is mainly dominated by Cu 3d and C 2p states, whereas the Cr 3d also has slight contribution to the HOMO. Figure 10d illustrates that the charge accumulation between the Cr and C atoms in the HOMO is much smaller than pure C−C bond,[30] meaning the weak bond strength. However, the charge distribution in the HOMO possesses a nodal structure between the Cu and C atoms, as shown in Figure 10e, indicating a presence of antibonding behavior, which induces the decrease of the bond strength and the stability of film seriously.

According to the above discussion, it can be concluded that Cu/Cr codoping modifies the structure of a-C film, resulting in the change of bond characteristics and DOS. Choi et al.[30] revealed that compared to the pure C−C covalent bond, the weak bond characteristics could lead to the small energy change caused by the distortion of bond structures. Because of the formed weak bond characteristics in Cu/Cr codoped a-C films, the codoped Cu and Cr atoms could play the role of a pivotal site to form the antibonding for Cu−C bond and the weak covalent bond for Cr−C bond and reduce the bond strength drastically, where the distortion of atomic bond structure can occur without the significant increase of the strain energy. Therefore, the relaxation of distorted C−C bond lengths and the formation of weak bond characteristics between the Cu/Cr and C atoms are supposed to be the fundamental reasons why the residual stress is significantly decreased due to the Cu/Cr codoping.

4. CONCLUSIONS

In this study, we first time brought forward the design of novel Cu/Cr codoped amorphous carbon films by employing ab initio calculations based on DFT. The dependence of residual stress upon the evolution of electronic structures induced by Cu/Cr codoping was studied. Compared with pure a-C film, Cu/Cr codoping could reduce the residual stress by 93.6% to 1.7 GPa as the Cu/Cr concentrations are 1.56 at. % and 1.56 at. %, respectively, whereas monodoping Cu or Cr into a-C films only decreased the residual stress by 78.5% to 5.7 or by 81.4 to 5.0 GPa. The structure analysis revealed that the codoping of Cu and Cr could relax the distorted bond lengths significantly. On the other hand, electronic structure calculation indicated a weak bonding interaction between the Cr and C atoms, whereas the antibonding interaction was observed for the Cu−C bonds, which could synergistically play a pivotal site to reduce the increase of strain energy change caused by the distortion of bond structure. These two factors are the key explain for the significant change of residual stress. Most importantly, our result provides a straightforward possibility by using the synergistic benefits from the binary doped metal feature to fabricate the new nanocomposite carbon-based films with high performance for the promising wider applications.

■ ASSOCIATED CONTENT

ⓈSupporting Information

The Supporting Information is available free of charge via the Internet at The Supporting Information is available free of charge on the ACS Publications website at DOI: 10.1021/acsami.5b09774.

> DOS and PDOS projected on the Cu or Cr atom in the Cu/Cr monodoped a-C film (PDF)

■ AUTHOR INFORMATION

Corresponding Authors

*Xiaowei Li. Tel: 86-574-86685036. Fax: 86-574-86685159. E-mail: lixw@nimte.ac.cn.

*Aiying Wang. Tel: 86-574-86685170. Fax: 86-574-86685159. E-mail: aywang@nimte.ac.cn.

Notes

The authors declare no competing financial interest.

■ ACKNOWLEDGMENTS

■ REFERENCES

(1) Robertson, J. Diamond-Like Amorphous Carbon. *Mater. Sci. Eng., R* **2002**, *37*, 129−281.

(2) Zhang, L.; Wei, X.; Lin, Y.; Wang, F. A Ternary Phase Diagram for Amorphous Carbon. *Carbon* **2015**, *94*, 202−213.

(3) Wang, L.; Zhang, R.; Jansson, U.; Nedfors, N. A Near-Wearless and Extremely Long Lifetime Amorphous Carbon Film under High Vacuum. *Sci. Rep.* **2015**, *5*, 11119−1−11119−13.

(4) Vetter, J. 60 Years of DLC Coatings: Historical Highlights and Technical Review of Cathodic Arc Processes to Synthesize Various DLC Types, and Their Evolution for Industrial Applications. *Surf. Coat. Technol.* **2014**, *257*, 213−240.

(5) Bewilogua, K.; Hofmann, D. History of Diamond-Like Carbon Films − From First Experiments to Worldwide Applications. *Surf. Coat. Technol.* **2014**, *242*, 214−225.

(6) Huang, J.; Wang, L.; Liu, B.; Wan, S.; Xue, Q. In Vitro Evaluation of the Tribological Response of Mo-Doped Graphite-Like Carbon Film in Different Biological Media. *ACS Appl. Mater. Interfaces* **2015**, *7*, 2772−2783.

(7) Wang, A. Y.; Lee, K. R.; Ahn, J. P.; Han, J. H. Structure and Mechanical Properties of W Incorporated Diamond-Like Carbon Films Prepared by a Hybrid Ion Beam Deposition Technique. *Carbon* **2006**, *44*, 1826−1832.

(8) Lee, C. S.; Lee, K. R.; Eun, K. Y.; Yoon, K. H.; Han, J. H. Structure and Properties of Si Incorporated Tetrahedral Amorphous Carbon Films Prepared by Hybrid Filtered Vacuum Arc Process. *Diamond Relat. Mater.* **2002**, *11*, 198−203.

(9) Dai, W.; Wang, A. Y. Deposition and Properties of Al-Containing Diamond-Like Carbon Films by a Hybrid Ion Beam Sources. *J. Alloys Compd.* **2011**, *509*, 4626−4631.

(10) Pang, X.; Shi, L.; Wang, P.; Xia, Y.; Liu, W. Influence of Methane Flow on the Microstructure and Properties of TiAl-Doped a-C:H Films Deposited by Middle Frequency Reactive Magnetron Sputtering. *Surf. Interface Anal.* **2009**, *41*, 924−930.

(11) Pang, X.; Hao, J.; Wang, P.; Xia, Y.; Liu, W. Effects of Bias Voltage on Structure and Properties of TiAl-Doped a-C:H Films Prepared by Magnetron Sputtering. *Surf. Interface Anal.* **2011**, *43*, 677−682.

(12) Pang, X.; Shi, L.; Wang, P.; Xia, Y.; Liu, W. Effects of Al Incorporation on the Mechanical and Tribological Properties of Ti-

Doped a-C:H Films Deposited by Magnetron Sputtering. *Curr. Appl. Phys.* **2011**, *11*, 771−775.

(13) Liu, X.; Yang, J.; Hao, J.; Zheng, J.; Gong, Q.; Liu, W. A Near-Frictionless and Extremely Elastic Hydrogenated Amorphous Carbon Film with Self-Assembled Dual Nanostructure. *Adv. Mater.* **2012**, *24*, 4614−4617.

(14) Zhang, R.; Wang, L.; Lu, Z. Probing the Intrinsic Failure Mechanism of Fluorinated Amorphous Carbon Film Based on the First-Principles Calculation. *Sci. Rep.* **2015**, *5*, 9419−1−9419−9.

(15) Li, X.; Ke, P.; Wang, A. Probing the Stress Reduction Mechanism of Diamond-Like Carbon Films by Incorporating Ti, Cr, or W Carbide-Forming Metals: Ab Initio Molecular Dynamics Simulation. *J. Phys. Chem. C* **2015**, *119*, 6086−6093.

(16) Kresse, G.; Furthmüller, J. Efficiency of Ab Initio Total Energy Calculations for Metals and Semiconductors Using Plane-Wave Basis Set. *Comput. Mater. Sci.* **1996**, *6*, 15−50.

(17) Kresse, G.; Furthmüller, J. Efficient Iterative Schemes for Ab Initio Total-Energy Calculations Using a Plane-Wave Basis Set. *Phys. Rev. B: Condens. Matter Mater. Phys.* **1996**, *54*, 11169−11186.

(18) Perdew, J. P.; Burke, K.; Ernzerhof, M. Generalized Gradient Approximation Made Simple. *Phys. Rev. Lett.* **1996**, *77*, 3865−3868.

(19) Zheng, B.; Zheng, W. T.; Zhang, K.; Wen, Q. B.; Zhu, J. Q.; Meng, S. H.; He, X. D.; Han, J. C. First-Principle Study of Nitrogen Incorporation in Amorphous Carbon. *Carbon* **2006**, *44*, 962−968.

(20) Bilek, M. M. M.; McKenzie, D. R.; McCulloch, D. G.; Goringe, C. M. Ab Initio Simulation of Structure in Amorphous Hydrogenated Carbon. *Phys. Rev. B: Condens. Matter Mater. Phys.* **2000**, *62*, 3071−3077.

(21) Gillan, M. J. Calculation of the Vacancy Formation Energy in Aluminum. *J. Phys.: Condens. Matter* **1989**, *1*, 689−711.

(22) Li, X.; Ke, P.; Wang, A. Stress Reduction of Cu-Doped Diamond-Like Carbon Films from Ab Initio Calculations. *AIP Adv.* **2015**, *5*, 017111−1−017111−9.

(23) Haerle, R.; Galli, G.; Baldereschi, A. Structural Models of Amorphous Carbon Surfaces. *Appl. Phys. Lett.* **1999**, *75*, 1718−1720.

(24) McCulloch, D. G.; McKenzie, D. R.; Goringe, C. M. Ab Initio Simulations of the Structure of Amorphous Carbon. *Phys. Rev. B: Condens. Matter Mater. Phys.* **2000**, *61*, 2349−2355.

(25) Chen, C. C.; Hong, F. C. N. Structure and Properties of Diamond-Like Carbon Nanocomposite Films Containing Copper Nanoparticles. *Appl. Surf. Sci.* **2005**, *242*, 261−269.

(26) McKenzie, D. R.; Muller, D.; Pailthorpe, B. A. Compressive Stress Induced Formation of Thin Film Tetrahedral Amorphous Carbon. *Phys. Rev. Lett.* **1991**, *67*, 773−776.

(27) Marks, N. A. Evidence for Subpicosecond Thermal Spikes in the Formation of Tetrahedral Amorphous Carbon. *Phys. Rev. B: Condens. Matter Mater. Phys.* **1997**, *56*, 2441−2446.

(28) Dai, W.; Ke, P.; Wang, A. Microstructure and Property Evolution of Cr-DLC Films with Different Cr Content Deposited by a Hybrid Beam Technique. *Vacuum* **2011**, *85*, 792−797.

(29) Li, X.; Ke, P.; Zheng, H.; Wang, A. Structural Properties and Growth Evolution of Diamond-Like Carbon Films with Different Incident Energies: a Molecular Dynamics Study. *Appl. Surf. Sci.* **2013**, *273*, 670−675.

(30) Choi, J. H.; Lee, S. C.; Lee, K. R. A First-Principles Study on the Bond Characteristics in Carbon Containing Mo, Ag, or Al Impurity Atoms. *Carbon* **2008**, *46*, 185−188.